Journal of Fluids and Structures 17 (2003) 147–161

JOURNAL OF FLUIDS AND STRUCTURES

www.elsevier.nl/locate/jnlabr/yjfls

Modal expansion of the perturbation velocity potential for a cantilevered fluid-conveying cylindrical shell

M.A. Langthjem*,[1], N. Olhoff

Institute of Mechanical Engineering, Aalborg University, Pontoppidanstræde 101, DK-9220 Aalborg East, Denmark

Received 13 August 2001; received in revised form 18 March 2002

Abstract

The subject of this paper is the application of the method of separation of variables and the Galerkin method for discretization of the equations of motion for a cantilevered cylindrical fluid-conveying shell. The perturbation velocity potential is expressed in terms of a series of orthonormal beam modal functions. The final Galerkin generalized fluid force coefficients are simple, compact, and easy to evaluate numerically. To validate the method, comparisons with results obtained from the Fourier transform method are made. Mismatch between the actual axial fluid modes and the assumed modes affects the Galerkin coefficients to some extent, but the unstable eigenvalue branch is only affected slightly over a wide range of system parameters, and critical flow speeds predicted by the two methods generally agree well.

1. Introduction

Fluid-conveying cylindrical shells are found in numerous industrial applications, in particular in connection with power generation (Au-Yang, 1985; Au-Yang, 2001). There are also numerous physiological applications, e.g., in connection with respiratory systems and blood flow (Pedley and Luo, 1998). The dynamics of fluid-conveying shells have thus been studied rather extensively. In practical applications, clamped–clamped boundary conditions are probably the most common. But cantilevered (clamped–free) shells are also found. For example, Fujita et al. (1991) mention a cantilever-type 'intermediate' heat exchanger in the reactor vessel of a fast breeder reactor. No direct support is added at one end because of large thermal expansion. But the main interest in cantilevered shells is probably as a model problem to study flow-induced dynamic instabilities due to the non-conservative character of the fluid forces (Païdoussis, 1987; Païdoussis and Li, 1993).

Analyses of complicated systems are commonly being based on the finite element method (Zienkiewicz and Taylor, 1991; Selmane and Lakis, 1997). In contrast, fundamental studies of simpler systems are often based on 'semi-analytical' discretization methods, such as power-series expansion (Niordson, 1953; Païdoussis and Denise, 1972), or the Galerkin method (Shayo and Ellen, 1978; Païdoussis, 1987) Four boundary conditions are specified at each end and accordingly, a power-series expansion is limited to eight wavenumbers. The Galerkin method is not subject to this restriction and may therefore give more accurate solutions.

Through the fundamental studies referred to up to this point, potential flow theory has proved to be adequate in yielding correct stability characteristics. The variables in the perturbation velocity potential Φ, expressed with respect to

*Corresponding author.
E-mail address: mikael@yz.yamagata-u.ac.jp (M.A. Langthjem).
[1] Present address: Department of Mechanical Systems Engineering, Faculty of Engineering, Yamagata University, 4-3-16, Jonan, Yonezawa, Yamagata 992-8510, Japan.

0889-9746/03/$ - see front matter
PII: S0889-9746(02)00113-5

Nomenclature

a	internal radius of the shell
A_j	linear combination factors for the modal expansion of the axial deflection, see Eq. (17)
$\mathbf{A}$	mass matrix defined by Eq. (59)
b_{ms}	coefficient defined by Eq. (38)
B_j	linear combination factors for the modal expansion of the circumferential deflection, see Eq. (17)
$\mathbf{B}$	fluid damping (Coriolis) matrix defined by Eq. (59)
c_{ms}	coefficient defined by Eq. (33)
$\mathbf{c}$	eigenvector for beam-mode oscillations, see Eq. (58)
C_j	linear combination factors for the modal expansion of the radial deflection, see Eq. (17)
$\mathbf{C}$	generalized stiffness matrix defined by Eq. (59)
d_{ms}	coefficient defined by Eq. (33)
$\mathbf{d}$	eigenvector for shell-mode oscillations, see Eq. (44)
D_j	linear combination factors for the perturbation velocity potential, see Eq. (25)
E_j	linear combination factors for the perturbation velocity potential, see Eq. (25)
f_j	beam expansion function (mode j)
$F_{u;v;w}$	differential operators for the shell equations
$\mathbf{F}$	complex system matrix defined by Eq. (45)
g_j	outflow function for the Fourier transform method, see Eq. (54)
H_j	linear combination factors for the perturbation velocity potential
i	$\sqrt{-1}$
I_n	modified Bessel function of first kind and of order n
$\mathbf{I}$	unit matrix
$\mathscr{I}_n$	a real, symmetric function defined by Eq. (53)
$\mathscr{I}_{mn}$	a real, symmetric function defined by Eq. (40)
k	wavenumber (continuous)
k_m	the mth (discrete) wavenumber
K_n	modified Bessel function of second kind and of order n
$\mathbf{K}$	stiffness matrix for beam-mode oscillations, see Eq. (58)
L	length of the shell
$Q_{msn}^{(j)}$	Galerkin fluid load coefficients defined by Eq. (49)
$Q_{msn}^{(j*)}$	Fourier–Galerkin fluid load coefficients defined by Eq. (52)
$\boldsymbol{Q}^{(j)}$	matrix with elements $Q_{msn}^{(j)}$ or $Q_{msn}^{(j*)}$
r	radius
R_m	radial expansion of perturbation velocity potential, given by Eq. (25)
t	time
T	time function, defined by Eq. (21)
u	axial deflection of the shell
U	undisturbed axial flow velocity
v	circumferential deflection of the shell
V_x	axial flow velocity by disturbed motion
V_θ	circumferential flow velocity by disturbed motion
V_r	radial flow velocity by disturbed motion
w	radial deflection of the shell
x	axial distance along the shell
X_m	axial expansion of perturbation velocity potential, defined by Eq. (30)
β	fluid mass parameter, defined by Eq. (57)
Γ_{mj}	outflow function for the Fourier transform method, see Eq. (54)
δ_{ms}	the Kronecker delta
Δ	the Laplacian operator, defined by Eq. (10)
θ	circumferential coordinate
Θ_n	part of the velocity potential which is a function of θ only
κ_j	eigenvalues corresponding to the beam expansion functions

λ	complex eigenvalues of the system matrix Eq. (60)
μ	mass parameter, defined by Eq. (48)
ρ	density of the fluid
Φ	perturbation velocity potential, given by Eq. (39)
Ψ	velocity potential, defined by Eq. (8)
ω	frequency

cylindrical polar coordinates (x, θ, r), can be separated by assuming solutions of the form

$$\Phi = \Phi(x, \theta, r, t) = R(r)X(x)\Theta(\theta)T(t), \tag{1}$$

where $R(r)$, $X(x)$, $\Theta(\theta)$, and $T(t)$ are functions of one variable only, and t is the time. The potential function Φ must satisfy the Laplace equation

$$\Delta\Phi = 0, \tag{2}$$

where Δ is the Laplacian. By virtue of the solution assumption (1) and simple assumptions regarding $\Theta(\theta)$ and $T(t)$, the partial differential equation (2) is split up into two ordinary differential equations, a modified Bessel equation in $R(r)$ (also including the circumferential mode number n) and a one-dimensional wave equation in $X(x)$,

$$X''(x) + k^2 X(x) = 0, \tag{3}$$

where k is a discrete wavenumber and a prime means differentiation with respect to the argument. By the power-series expansion method, the assumption $X(x) = C\exp(\mathrm{i}kx)$ is applied, C being a constant, and each term satisfies (3) for all possible sets of boundary conditions.

Modal expansion of $X(x)$ and the structural deflections is straightforward in the pinned–pinned case and works well in connection with the Galerkin method, as the fluid and structural modes are orthogonal, see, e.g., Chen (1972). The situation is more complicated when clamped ends are involved. In such cases the potential has previously been discretized by application of Fourier transform (Shayo and Ellen, 1978; Païdoussis et al., 1986). A less restrictive variable separation is then used in the Laplace equation, namely

$$\Phi(x, \theta, r, t) = \mathscr{R}(r, x)\Theta(\theta)T(t) \tag{4}$$

and the r and x variables are separated in the Fourier domain by applying the Fourier transform couple

$$\mathscr{R}^*(r, k) = \int_{-\infty}^{\infty} \mathscr{R}(r, x)\mathrm{e}^{\mathrm{i}kx}\,\mathrm{d}x, \quad \mathscr{R}(r, x) = \frac{1}{2\pi}\int_{-\infty}^{\infty} \mathscr{R}^*(r, k)\mathrm{e}^{-\mathrm{i}kx}\,\mathrm{d}k, \tag{5}$$

where k here is a continuously varying wavenumber.

Dowell and Widnall (1966a) and Widnall and Dowell (1967) introduced the use of Fourier transform to calculate the generalized aerodynamic forces on oscillating cylindrical shells. External flow was considered in Dowell and Widnall (1966a) and internal flow in Widnall and Dowell (1967). [Fourier transform is needed for subsonic flow, while both Laplace and Fourier transforms work for supersonic flow. See also Dowell and Widnall (1966b) for the supersonic case.] The Fourier transform was also applied by Shayo and Ellen (1974) in a study of the stability of simply supported shells containing a flowing fluid, and by Au-Yang (1977) and Païdoussis et al (1984) in connection with fluid-containing and fluid-conveying coaxial shells.

A drawback of the Fourier transform approach is that the integrals most often only can be evaluated numerically. And for the case of a cantilevered shell, a model of the jet issuing from the free end also needs to be included. This is because the Fourier transform basically expands each structural modal function f_m into fluid modal functions, whereby the fulfillment of the natural boundary conditions $\partial^2 f_m/\partial x^2 = 0$ and $\partial^3 f_m/\partial x^3 = 0$ at the free end is lost.

The primary goal of the present paper is to derive simple, approximate expressions for the generalized fluid forces, based on a Galerkin discretization of the coupled fluid–structure problem where both the structural deflections and the fluid perturbation pressure are expanded in the same set of orthonormal beam modal functions. The problem is posed as a boundary value problem. To carry this through, it will be accepted that Eq. (3) is not satisfied exactly, but only approximately, in the averaged, 'weak' form of the Galerkin method. This is because the fulfillment of the (structural) natural boundary conditions at the free end is given higher priority than satisfying the Laplace equation (2) exactly. A downstream jet model is unnecessary, as the behavior of the jet is related to the structure through the fluid boundary conditions.

The work is divided into seven sections. Section 2 outlines the governing equations and boundary conditions for the shell and the fluid. In Section 3, equations are derived for the perturbation velocity potential and the perturbation pressure acting on the wall of the shell. In Section 4, the Galerkin generalized fluid force coefficients are given. Section 5 gives the Galerkin coefficients based on the Fourier transform method and outlines the numerical evaluation. In Section 6 comparisons of Galerkin coefficients and beam mode critical flow speed predictions are made. Finally, some concluding remarks are made in Section 7.

The paper also includes two appendices. In Appendix A, the beam modal expansion functions are listed. Appendix B is concerned with a specific mathematical detail.

2. Equations of motion and boundary conditions

Let U be the uniform entrance velocity of an incompressible inviscid fluid of density ρ, flowing steadily in the axial direction within a flexible cylindrical shell of radius a. The fluid is entering at $x=0$ and discharging at $x=L$. Small vibrations of the shell around its equilibrium position is described by a set of three coupled partial differential equations, written symbolically here as

$$F_u(u,v,w)=0,\quad F_v(u,v,w)=0,\quad F_w(u,v,w)=0, \tag{6}$$

where the deflections (u,v,w) are given with respect to cylindrical polar coordinates (x,θ,r). The full equations will not be considered here, but can be found in e.g., Païdoussis and Denise (1972) and Shayo and Ellen (1978). The boundary conditions for the cantilevered shell are

$$u=v=w=0 \quad \text{and} \quad \partial w/\partial x=0 \quad \text{at} \quad x=0;$$

$$\left.\begin{array}{r}\text{Normal force}\\ \text{Bending moment}\\ \text{Effective shear force}\\ \text{Effective membrane shear force}\end{array}\right\}=0 \quad \text{at} \quad x=L. \tag{7}$$

For mathematical expressions for the conditions at $x=L$, see again Païdoussis and Denise (1972) and Shayo and Ellen (1978).

The velocity potential for the fluid is defined as

$$\Psi = Ux+\Phi, \tag{8}$$

where Φ is a perturbation velocity potential. The fluid velocities in a disturbed state are given by

$$V_x=\frac{\partial\Psi}{\partial x}=U+\frac{\partial\Phi}{\partial x};\quad V_\theta=\frac{1}{r}\frac{\partial\Psi}{\partial\theta}=\frac{1}{r}\frac{\partial\Phi}{\partial\theta};\ V_r=\frac{\partial\Psi}{\partial r}=\frac{\partial\Phi}{\partial r}. \tag{9}$$

The perturbation potential Φ must satisfy the Laplace equation

$$\frac{1}{r}\frac{\partial}{\partial r}\left(r\frac{\partial\Phi}{\partial r}\right)+\frac{1}{r^2}\frac{\partial^2\Phi}{\partial\theta^2}+\frac{\partial^2\Phi}{\partial x^2}=0. \tag{10}$$

Knowing the potential, the perturbation pressure on the pipe wall is evaluated from the linearized Bernoulli equation as

$$p=-\rho\left(\frac{\partial\Phi}{\partial t}+U\frac{\partial\Phi}{\partial x}\right) \text{ at } r=a. \tag{11}$$

The kinematic boundary condition, to be satisfied on the pipe wall, is

$$\frac{\partial\Phi}{\partial r}=\frac{\partial w}{\partial t}+U\frac{\partial w}{\partial x} \text{ at } r=a. \tag{12}$$

The inflow boundary condition for the fluid is specified as follows:

$$V_x=U \text{ at } x=0, \quad \text{i.e.,} \qquad \frac{\partial\Phi}{\partial x}=0 \text{ at } x=0. \tag{13}$$

The perturbation pressure p vanishes at the free end. Eq. (11) then gives the outflow boundary condition

$$\frac{\partial\Phi}{\partial x}=-\frac{1}{U}\frac{\partial\Phi}{\partial t}=-\mathrm{i}\frac{\omega}{U}\Phi \text{ at } x=L, \tag{14}$$

assuming a time dependence $\exp(\mathrm{i}\omega t)$. It will be assumed in the present paper that $|\Phi\omega/U| \ll |U|$ at $x = L$, by which the non-dimensional perturbation velocity $|U^{-1}\partial\Phi/\partial x| \ll 1$. Then, based on the approximation $U^{-1}\partial\Phi/\partial x \approx 0$ at $x = L$, Eq. (14) is simplified to

$$\frac{\partial\Phi}{\partial x} = 0 \text{ at } x = L. \tag{15}$$

Finally, the potential must also satisfy the singularity condition

$$\Phi < \infty \text{ at } r = 0. \tag{16}$$

3. Separation of variables

3.1. Deflections

As in Shayo and Ellen (1978), the deflections (u, v, w) are expanded as

$$\begin{Bmatrix} u \\ v \\ w \end{Bmatrix} = \exp(\mathrm{i}\omega t) \sum_{m=1}^{\infty} \begin{Bmatrix} A_m \cos(n\theta) a\partial f_m(x)/\partial x \\ B_m \sin(n\theta) f_m(x) \\ C_m \cos(n\theta) f_m(x) \end{Bmatrix}, \tag{17}$$

where A_m, B_m and C_m are constants (linear combination factors). The expansion functions $f_m(x)$ are the eigenfunctions for a vibrating beam, given by

$$f_m(x) = \zeta_m^{(1)} \sin(\kappa_m x) + \zeta_m^{(2)} \cos(\kappa_m x) + \zeta_m^{(3)} \sinh(\kappa_m x) + \zeta_m^{(4)} \cosh(\kappa_m x). \tag{18}$$

The eigenvalues κ_m and the constants $\zeta_m^{(j)}$ are determined by the boundary conditions. Numerical values for the clamped–free case are given in Appendix A. The beam functions are normalized such that

$$\frac{1}{L}\int_0^L f_m f_j \,\mathrm{d}x = \delta_{mj} = \begin{cases} 1 \text{ for } m = j, \\ 0 \text{ for } m \neq j. \end{cases} \tag{19}$$

3.2. Velocity potential

The potential Φ_n, corresponding to the nth circumferential mode, is assumed to have the form

$$\Phi_n = \sum_{m=1}^{\infty} \Phi_{mn}, \quad \Phi_{mn}(x, \theta, r, t) = R_m(r) X_m(x) \Theta_n(\theta) T(t), \tag{20}$$

with

$$\Theta_n(\theta) = \cos(n\theta), \quad T(t) = \exp(\mathrm{i}\omega t). \tag{21}$$

Inserting Eqs. (20) and (21) into (10) gives

$$\sum_{m=1}^{\infty} \left[\frac{\partial^2 R_m}{\partial r^2} X_m + \frac{1}{r}\frac{\partial R_m}{\partial r} X_m - \frac{n^2}{r^2} R_m X_m + R_m \frac{\partial^2 X_m}{\partial x^2} \right] = 0, \tag{22}$$

which can be separated into the following equations (Courant and Hilbert, 1953, Chapter V):

$$\frac{\partial^2 R_m}{\partial r^2} + \frac{1}{r}\frac{\partial R_m}{\partial r} - \left(\frac{n^2}{r^2} + k_m^2 \right) R_m = 0, \tag{23}$$

$$\frac{\partial^2 X_m}{\partial x^2} + k_m^2 X_m(x) = 0, \quad m = 1, 2, \ldots, \infty, \tag{24}$$

where k_m is the mth eigenvalue.

The general solution to the modified Bessel equation (23) is

$$R_m(r) = D_m \mathrm{I}_n(k_m r) + E_m \mathrm{K}_n(k_m r) \tag{25}$$

where D_m and E_m are constants, and I_n and K_n are modified Bessel functions of first and second kind, respectively, and of order n. But in order to satisfy Eq. (16), $E_m \equiv 0$.

The general solution to the wave equation (24) is given by

$$X_m(x) = \mathscr{A}_m \sin(k_m x) + \mathscr{B}_m \cos(k_m x), \tag{26}$$

and by imposing the boundary conditions (13) and (15), which in terms of X_m take the form

$$\frac{\partial X_m}{\partial x} = 0 \quad \text{for} \quad x = 0 \quad \text{and} \quad L, \tag{27}$$

the eigensolutions are determined as

$$X_m(x) = \mathscr{B}_m \cos(k_m x), \;\; k_m L = m\pi. \tag{28}$$

The eigenfunctions can be expanded in the orthonormal beam functions $f_m(x)$ as

$$\cos(k_m x) = \sum_{j=1}^{\infty} H_{mj} f_j(x), \;\; H_{mj} = \frac{1}{L}\int_0^L \cos(k_m x) f_j(x)\,\mathrm{d}x. \tag{29}$$

It may be expected that a good number of terms will be needed to yield convergent results, as the expansion functions $f_j(x)$ do not satisfy the boundary conditions (27). In the present paper, rather than using Eq. (29), the $X_m(x)$ functions are taken, at the outset, as

$$H_m f_m(x), \tag{30}$$

where H_m are constants, and eigenvalues k_m are obtained from the Galerkin equations

$$\sum_{m=1}^{\infty} H_m \int_0^L \{f_m'' f_j + k_m^2 f_m f_j\}\,\mathrm{d}x = 0, \quad j = 1, 2, \ldots, \tag{31}$$

which is obtained as the weak form of Eq. (24) with Eq. (30) inserted. (A prime indicates differentiation with respect to the argument x.) When imposing the boundary conditions (27), (31) takes the form

$$\sum_{m=1}^{\infty} H_m \int_0^L \left\{f_m' f_j' - k_m^2 f_m f_j\right\}\mathrm{d}x = 0, \;\; j = 1, 2, \ldots. \tag{32}$$

By using Eq. (19) and the notation

$$c_{mj} = \frac{1}{L}\int_0^L f_m'' f_j\,\mathrm{d}x, \;\; d_{mj} = \frac{1}{L}\int_0^L f_m' f_j'\,\mathrm{d}x = \frac{1}{L}[f_m' f_j]_{x=L} - c_{mj}, \tag{33}$$

Eq. (32) can be written as

$$\begin{bmatrix} d_{11} - k_1^2 & d_{12} & d_{13} & \cdots \\ d_{21} & d_{22} - k_2^2 & d_{23} & \cdots \\ d_{31} & d_{32} & d_{33} - k_3^2 & \cdots \\ \vdots & \vdots & \vdots & \ddots \end{bmatrix} \begin{Bmatrix} H_1 \\ H_2 \\ H_2 \\ \vdots \end{Bmatrix} = \begin{Bmatrix} 0 \\ 0 \\ 0 \\ \vdots \end{Bmatrix}. \tag{34}$$

The wavenumbers k_m are thus determined as the square root of the eigenvalues of the matrix with elements d_{mj}. As this matrix is symmetric and positive definite, all eigenvalues are positive. Eq. (34) is basically the Rayleigh–Ritz method by Kamke's quotient (rather than Rayleigh's quotient) as the boundary conditions (27) are not satisfied by the expansion functions $f_m(x)$, but incorporated through integration by parts (Kamke, 1967, Chapter B, Section 1). Païdoussis and Issid (1974) and Païdoussis (1998) give analytical expressions for the coefficients c_{mj}. For completeness, these expressions are also included in Appendix A.

Writing the velocity potential as

$$\Phi_n = \sum_{m=1}^{\infty} D_m \mathrm{I}_n(k_m r) f_m(x) \cos(n\theta)\mathrm{e}^{\mathrm{i}\omega t}, \tag{35}$$

the boundary condition (12) gives

$$\frac{\partial}{\partial r}\left\{\sum_{j=1}^{\infty} D_j \mathrm{I}_n(k_j r) f_j(x)\right\}_{r=a} = \sum_{j=1}^{\infty} C_j\left\{\mathrm{i}\omega f_j(x) + U f_j'(x)\right\}. \tag{36}$$

By multiplying both sides by $f_m(x)$ and integrating from 0 to L, the constants D_m are obtained as

$$D_m = \frac{\mathrm{i}\omega C_m + U\sum_j b_{jm} C_j}{k_m \mathrm{I}_n'(k_m a)}, \tag{37}$$

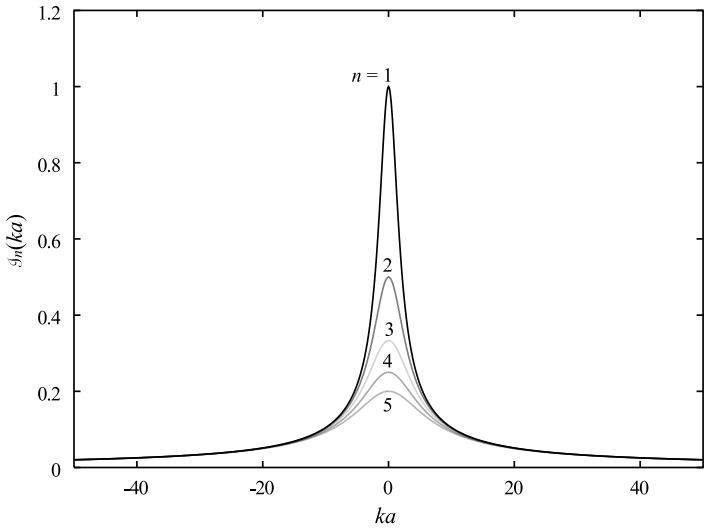

Fig. 1. The function $\mathscr{I}_{mn}(k_m a)$ defined by Eq. (40). [It is equivalent to $\mathscr{I}_n(ka)$ defined by Eq. (53), but Eq. (40) is defined for discrete k_m-values, while Eq. (53) is for continuously varying k.]

where a prime indicates differentiation with respect to the argument. To obtain Eq. (37), it has been used that

$$f'_m(x) = \sum_{j=1}^{\infty} b_{mj} f_j(x), \quad b_{mj} = \frac{1}{L}\int_0^L f'_m f_j \, \mathrm{d}x. \tag{38}$$

The final expression for the velocity potential is

$$\Phi_n = a\mathrm{e}^{\mathrm{i}\omega t}\cos(n\theta)\sum_{m=1}^{\infty} C_m \left[\mathrm{i}\omega \mathscr{I}_{mn} f_m + U\left\{\sum_{j=1}^{\infty} b_{mj} f_j \mathscr{I}_{jn}\right\}\right], \tag{39}$$

where

$$\mathscr{I}_{mn} = \frac{\mathrm{I}_n(k_m a)}{k_m a \mathrm{I}'_n(k_m a)}. \tag{40}$$

Using Eq. (11) with Eq. (39) inserted, the pressure on the pipe wall can be expressed as

$$p_n = \sum_{m=1}^{\infty} p_{mn} = -\rho a \mathrm{e}^{\mathrm{i}\omega t}\cos(n\theta)\sum_{m=1}^{\infty} C_m \left[-\omega^2 \mathscr{I}_{mn} f_m + \mathrm{i}\omega U\left\{\mathscr{I}_{mn} f'_m + \sum_{j=1}^{\infty} b_{mj} f_j \mathscr{I}_{jn}\right\} + U^2 \sum_{j=1}^{\infty} b_{mj} f'_j \mathscr{I}_{jn}\right]. \tag{41}$$

It may be noted that $\mathrm{I}'_n(z) = \mathrm{I}_{n+1}(z) + \mathrm{I}_n(z)\ n/z$ and, by using the power series for I_n and I_{n+1}, that

$$\mathscr{I}_{mn} = \frac{1}{n}\left\{1 - \frac{a^2 k_m^2}{2n(n+1)} + \mathscr{O}(a^4 k_m^4)\right\}. \tag{42}$$

This is a real, even function in ak_m, as may be seen also from Fig. 1, which shows the 'full' function, as given by Eq. (40).

4. Discretization of the shell equations

The discretization follows the standard Galerkin approach. The residual equations are

$$\int_0^{2\pi}\int_0^L f_s \cos(n\theta)\{F_u \ F_v \ F_w\}^{\mathrm{T}} \, \mathrm{d}x \, \mathrm{d}\theta = \{0 \ 0 \ 0\}^T,$$
$$s = 1, 2, \ldots, \infty. \tag{43}$$

The eigenmode expansions (17) for u, v w are now inserted into the differential equations (6). Truncating the infinite series after S terms ($m, s = 1, 2, \ldots, S$) leads to a linear equation system of the form

$$\mathbf{Fd} = \mathbf{0}. \tag{44}$$

Here $\mathbf{d} = \{A_1, \ldots, A_S, B_1, \ldots, B_S, C_1, \ldots, C_S\}^{\mathrm{T}}$ is the vector of linear combinations factors, and $\mathbf{F}$ is a $3S \times 3S$ complex matrix which has the form

$$\mathbf{F} = -\omega^2 \mathbf{F}_2 + 2\mathrm{i}\omega U \mathbf{F}_1 + U^2 \mathbf{F}_0. \tag{45}$$

The generalized fluid force coefficients entering in this equation system take the form

$$C_m \, \mathrm{e}^{\mathrm{i}\omega t} Q_{msn} = -\int_0^{2\pi} \int_0^L \cos(n\theta) p_{mn} f_s \, \mathrm{d}x \, \mathrm{d}\theta = C_m \mathrm{e}^{\mathrm{i}\omega t} \int_0^{2\pi} \cos^2(n\theta) \, \mathrm{d}\theta \rho a \times \int_0^L \left[-\omega^2 \mathscr{I}_{mn} f_m f_s + \mathrm{i}\omega U \left\{ \sum_{j=1}^{\infty} b_{mj} \mathscr{I}_{jn} f_j f_s + \mathscr{I}_{mn} f'_m f_s \right\} + U^2 \sum_{j=1}^{\infty} b_{mj} \mathscr{I}_{jn} f'_j f_s \right] \mathrm{d}x. \tag{46}$$

To conform with Eq. (45) the factors Q_{msn} are split into three parts, such that

$$Q_{msn} = -\omega^2 \mu Q^{(1)}_{msn} + 2\mathrm{i}\omega U \mu Q^{(2)}_{msn} + U^2 \mu Q^{(3)}_{msn}, \tag{47}$$

where

$$\mu = \rho \pi a^2 / \bar{a} \tag{48}$$

and

$$Q^{(1)}_{msn} = \mathscr{I}_{mn} \delta_{ms}, \quad Q^{(2)}_{msn} = \tfrac{1}{2}(\mathscr{I}_{mn} + \mathscr{I}_{sn}) b_{ms}, \quad Q^{(3)}_{msn} = \sum_j \mathscr{I}_{jn} b_{mj} b_{js}. \tag{49}$$

The three terms $Q^{(j)}_{msn}$, $j = 1, 2, 3$, in Eq. (49) correspond to: (1) added mass; (2) fluid damping; and (3) follower-type centrifugal force, respectively.

Nondimensional 'overbarred' quantities are defined as

$$\bar{k}_m = L k_m, \quad \bar{x} = x/L, \quad \bar{a} = a/L. \tag{50}$$

By using Eq. (42) it is immediately seen that if $\bar{k}_m = O(1)$, $\bar{a} \ll 1$, and $n \neq 0$ (not 'breathing mode' oscillations) then $\mathscr{I}_{mn} \approx 1/n$ and Eq. (49) reduces to the 'plug flow result' (Dowell and Widnall, 1966a; Païdoussis et al., 1986)

$$Q^{(1)}_{msn} = \delta_{ms}/n, \quad Q^{(2)}_{msn} = b_{ms}/n, \quad Q^{(3)}_{msn} = c_{ms}/n. \tag{51}$$

The result $\sum_j b_{mj} b_{js} = c_{ms}$ is shown in Appendix B. It should also be noted that the coefficients $Q^{(j)}_{msn}$, $j = 1, 2, 3$, of Eq. (49) have the same symmetry properties as the plug flow coefficients of Eq. (51). The term $Q^{(3)}_{msn}$ is rapidly converging in any of the numerical cases considered (see Section 6). An example of convergence history, for $m = s = 4$, $n = 1$, and $\bar{a} = 0.25$, is shown in Fig. 2.

5. The Fourier transform method

To validate the main results Eq. (49), they will be compared with those obtained by the Fourier transform method. Following Shayo and Ellen (1978); Païdoussis et al. (1986) and Païdoussis (1998), the Fourier representation of $Q^{(j)}_{msn}$, $j = 1, 2, 3$, is given by

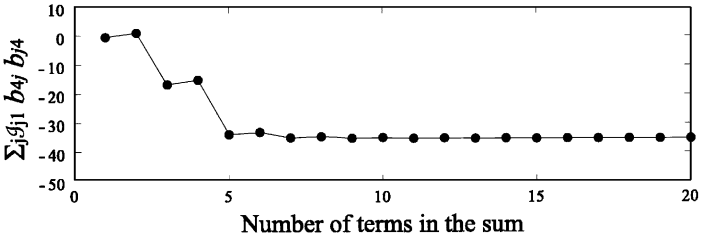

Fig. 2. Convergence of the term $Q^{(3)}_{msn} = \sum_j \mathscr{I}_{jn} b_{mj} b_{js}$, Eq. (49). The case shown is for $m = s = 4$, $n = 1$, and $a/L = 0.25$.

$$Q_{msn}^{(1*)} = \frac{1}{2\pi}\int_{-\infty}^{\infty} \mathscr{I}_n \left\{ \int_0^1 f_m e^{i\bar{k}\bar{x}}\,d\bar{x} + \int_1^{\infty} g_m e^{i\bar{k}\bar{x}}\,d\bar{x} \right\} \left\{ \int_0^1 f_s e^{-i\bar{k}\bar{x}}\,d\bar{x} \right\} d\bar{k},$$

$$Q_{msn}^{(2*)} = -\frac{i}{2\pi}\int_{-\infty}^{\infty} \bar{k}\mathscr{I}_n \left\{ \int_0^1 f_m e^{i\bar{k}\bar{x}}\,d\bar{x} + \int_1^{\infty} g_m e^{i\bar{k}\bar{x}}\,d\bar{x} \right\} \left\{ \int_0^1 f_s e^{-i\bar{k}\bar{x}}\,d\bar{x} \right\} d\bar{k},$$

$$Q_{msn}^{(3*)} = -\frac{1}{2\pi}\int_{-\infty}^{\infty} \bar{k}^2\mathscr{I}_n \left\{ \int_0^1 f_m e^{i\bar{k}\bar{x}}\,d\bar{x} + \int_1^{\infty} g_m e^{i\bar{k}\bar{x}}\,d\bar{x} \right\} \left\{ \int_0^1 f_s e^{-i\bar{k}\bar{x}}\,d\bar{x} \right\} d\bar{k}, \tag{52}$$

where $g_m(\bar{x})$ is a so-called 'outflow model', and

$$\mathscr{I}_n = \frac{I_n(ka)}{ka I_n'(ka)}. \tag{53}$$

One possible outflow model function $g_m(\bar{x})$ is given by Nguyen et al. (1993) as

$$g_m(\bar{x}) = (\Gamma_{m1}\bar{x} + \Gamma_{m2})e^{1-\bar{x}},\ \ \Gamma_{m1} = [f_m + f_m']_{\bar{x}=1}, \Gamma_{m2} = -[f_m']_{\bar{x}=1}. \tag{54}$$

This model has the properties

$$\text{(i)}\ [g_m(\bar{x})]_{\bar{x}=1} = [f_m(\bar{x})]_{\bar{x}=1},\ \ \text{(ii)}\ \ [g_m'(\bar{x})]_{\bar{x}=1} = [f_m'(\bar{x})]_{\bar{x}=1},$$

$$\text{(iii)}\ \ [g_m(\bar{x})]_{\bar{x}\to\infty} = 0,\ \ \text{(iv)}\ \ [g_m'(\bar{x})]_{\bar{x}\to\infty} = 0, \tag{55}$$

and the terms $Q_{msn}^{(j*)}$, $j = 1, 2, 3$, converge. The integral of the outflow model function is evaluated as

$$\int_1^{\infty} g_m e^{i\bar{k}\bar{x}}\,d\bar{x} = \frac{e^{i\bar{k}}}{(-1+i\bar{k})^2}\{2\Gamma_{m1} + \Gamma_{m2} - i\bar{k}(\Gamma_{m1} + \Gamma_{m2})\}. \tag{56}$$

The other two 'inner' integrals are also evaluated analytically, but the resulting expressions are too long to be of interest. The 'outer' integration, running over $-\infty < \bar{k} < \infty$, is performed numerically. The infinite interval of integration is replaced by a finite one, sufficiently large to ensure convergence of the resulting coefficients (52). The finite interval is divided into a number of sub-intervals wherein the integrations are performed by using a 10-point Gauss–Legendre method (Press et al. 1992). In all numerical results presented in the following, the range $-1000 < \bar{k} < 1000$ split up into 1000 subintervals was used.

6. Comparison of numerical results by the two methods

6.1. Galerkin generalized fluid load coefficients

To examine the agreement between the modal expansion (ME) method and the Fourier transform (FT) method, the Galerkin generalized fluid force coefficients $Q_{msn}^{(j)}$ and $Q_{msn}^{(j*)}$ will be compared for several values of the modal numbers m and s. The results have been checked for several values of the circumferential wavenumber n, but only those for $n = 1$ will be displayed here, as the results are qualitatively similar for other values of n.

The results are shown in Fig. 3. The solid curves give the results of the present ME method, while the results of the FT method are given by □ for the added mass coefficients, by ∇ for the fluid damping coefficients, and by ○ for the centrifugal force coefficients. Parts (a)–(d) show the first four diagonal elements $(m, s) = (1, 1), \ldots, (4, 4)$. It is noticed that the agreement between the centrifugal force coefficients is very poor for $(m, s) = (1, 1)$ and that the agreement is getting better and better for increasing modal number. This is because the first modal function $f_1(x)$ is far from being able to resemble the true eigenfunction (28) to the wave equation (24), but the mismatch becomes less severe with increasing modal number, as the modal functions become more and more 'sinuous'.

The off-diagonal terms, shown in parts (e)–(h), generally agree reasonably well. But in any case the ME method predicts an increase in the absolute value of the centrifugal force coefficients when the slenderness ratio $\bar{a}$ is increased from zero to a moderate value (approximately between 0.1 and 0.2) and then a decrease by further increase of $\bar{a}$. This is not a general trend by the FT method, and the cases where these terms have continuously decreasing absolute values are where the largest discrepancies between the results of the two methods are found.

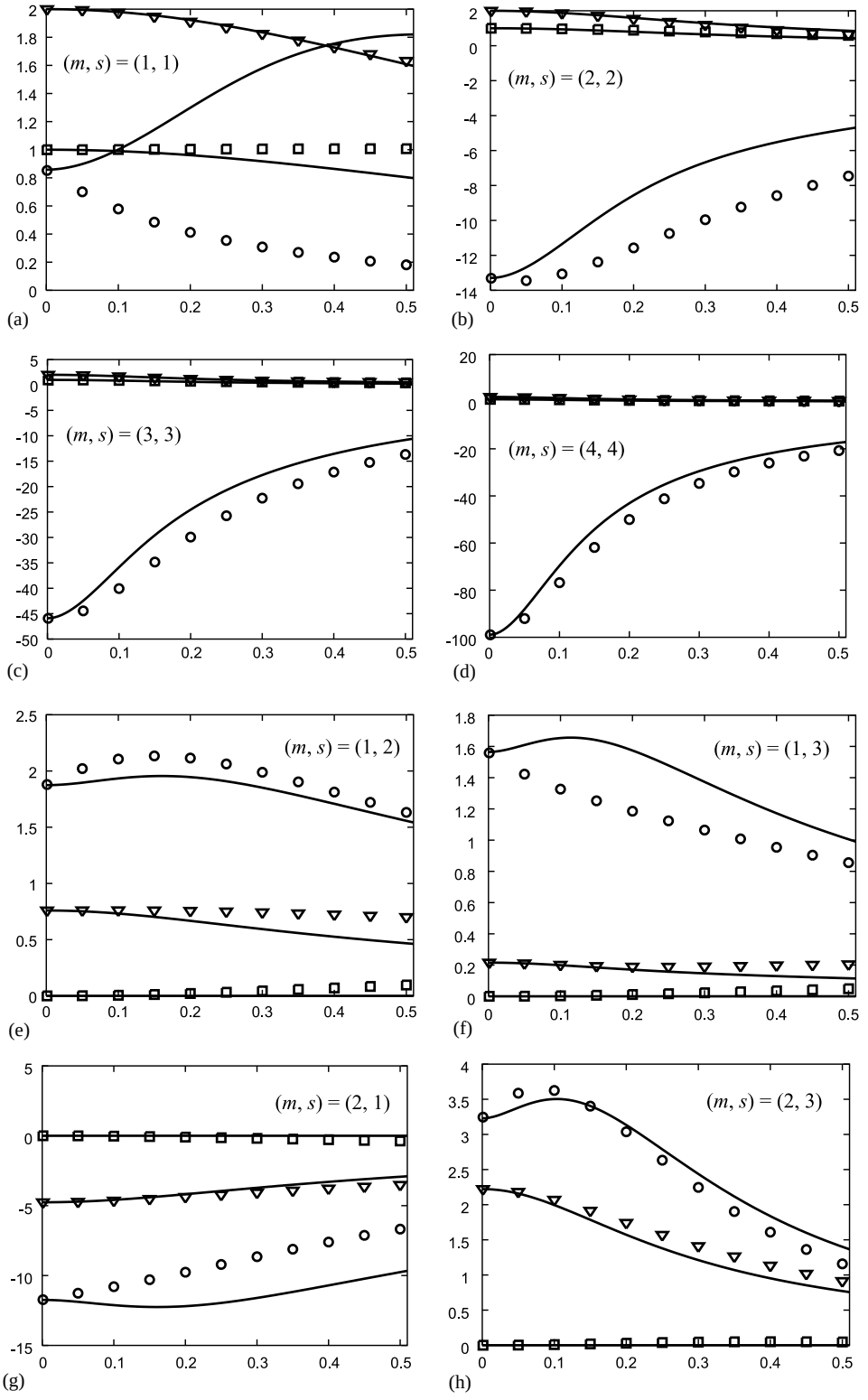
(m, s) = (1, 1)
(a)
(m, s) = (2, 2)
(b)
(m, s) = (3, 3)
(c)
(m, s) = (4, 4)
(d)
(m, s) = (1, 2)
(e)
(m, s) = (1, 3)
(f)
(m, s) = (2, 1)
(g)
(m, s) = (2, 3)
(h)
a/L

6.2. Beam mode flutter calculations

In order to check the influence on dynamic stability of the disagreements between the Galerkin generalized fluid force coefficients $Q^{(j)}_{msn}$ and $Q^{(j*)}_{msn}$, some calculations will be made for the beam mode oscillations, i.e., for $n = 1$. This means that only deflections w in radial direction will be considered. As the focus point of this paper is on the fluid-dynamical modelling, the influence of shear deformation on the tube dynamics will be ignored, although this may be of significance in cases of short, 'stubby' tubes. It must also be mentioned that higher shell modes ($n > 1$) may be predominant in many practical cases.

6.2.1. Theory

Writing the matrices with elements $Q^{(j)}_{ms1}$ (or $Q^{(j*)}_{ms1}$) as $\mathbf{Q}^{(j)}$, and introducing the nondimensional parameters

$$\bar{U} = UL\sqrt{\frac{\text{fluid mass per unit length}}{\text{bending stiffness}}},$$

$$\beta = \frac{\text{fluid mass per unit length}}{\text{total mass per unit length}}, \tag{57}$$

$$\bar{\omega} = \omega L^2\sqrt{\frac{\text{total mass per unit length}}{\text{bending stiffness}}},$$

the equation of motion can be written as the $S \times S$ matrix equation

$$[-\bar{\omega}^2\{(1-\beta)\mathbf{I} + \beta\mathbf{Q}^{(1)}\} + \mathrm{i}\bar{\omega}2\bar{U}\sqrt{\beta}\mathbf{Q}^{(2)} + \mathbf{K} + \bar{U}^2\mathbf{Q}^{(3)}]\mathbf{c} = \mathbf{0}, \tag{58}$$

where the structural mass matrix $\mathbf{I}$ simply is the unit matrix. The stiffness matrix $\mathbf{K} = \mathrm{diag}[\kappa_1^4\ \kappa_2^4\ \cdots\ \kappa_S^4]$ and the eigenvector $\mathbf{c} = \{C_1\ C_2\ \cdots\ C_S\}^{\mathrm{T}}$. By introducing the matrices

$$\mathbf{A} = (1-\beta)\mathbf{I} + \beta\mathbf{Q}^{(1)},\ \mathbf{B} = 2\bar{U}\sqrt{\beta}\mathbf{Q}^{(2)}, \mathbf{C} = \mathbf{K} + \bar{U}^2\mathbf{Q}^{(3)}, \tag{59}$$

the equation system (58) can be rewritten as the $2S \times 2S$ matrix eigenvalue problem

$$\mathrm{i}\bar{\omega}\begin{Bmatrix} \mathrm{i}\bar{\omega}\mathbf{c} \\ \mathbf{c} \end{Bmatrix} = \begin{bmatrix} -\mathbf{A}^{-1}\mathbf{B} & -\mathbf{A}^{-1}\mathbf{C} \\ \mathbf{I} & \mathbf{0} \end{bmatrix}\begin{Bmatrix} \mathrm{i}\bar{\omega}\mathbf{c} \\ \mathbf{c} \end{Bmatrix}. \tag{60}$$

The stability analysis is performed by determining the complex eigenvalues $\lambda = \lambda_R \pm \mathrm{i}\lambda_I$ of the real system matrix defined on the right-hand side of Eq. (60). Dynamic instability (flutter) is initiated when an eigenvalue with nonzero imaginary part λ_I gets a positive real part ($\lambda_R > 0$). Static instability (divergence) is initiated when a complex eigenvalue becomes real and positive. The instability is always of the dynamic type for the cantilevered tube (Païdoussis, 1998). The eigenvalues are found numerically by using the QR method (Press et al., 1992). The values of the flow speed $\bar{U}$ defining the instability boundaries are determined using a bisection method.

6.2.2. Numerical examples

Stability curves depicting critical flow speed as function of the slenderness ratio $\bar{a}$ are shown in Fig. 4 for (a) $\beta = 0.2$, (b) $\beta = 0.5$, and (c) $\beta = 0.8$. Ten modal functions ($S = 10$) were applied in all calculations. The convergence histories shown in Table 1 indicate that this will give results with three significant digits. However, computations with $S > 10$ were only done for the ME method, not for the FT method. [Two modes only ($S = 2$) cannot give meaningful results for $\beta = 0.8$. Those results are therefore not included in the table.]

The solid curves depict the results of the ME method, while the dots are the results of the FT method. Considering the disagreement between some of the Galerkin coefficients obtained by the two methods, the agreement between the critical flow speed predictions appear to be surprisingly good in any case. It may be remarked that the 'wrong' trend of

Fig. 3. Comparison between the generalized fluid force coefficients $Q^{(j)}_{msn}$ (49) obtained by the present method, and $Q^{(j*)}_{msn}$ (52) obtained by the Fourier transform method: □, the added mass coefficients $Q^{(1*)}_{msn}$; ∇, the fluid damping coefficients $Q^{(2*)}_{msn}$; ○, the fluid loading coefficient $Q^{(3*)}_{msn}$. The coefficients $Q^{(j)}_{msn}, j = 1, 2, 3$, are shown with full lines. All results are for $n = 1$. Note that the two methods give coinciding results for $a/L \to 0$ (the 'plug flow limit'). (a) $m = s = 1$; (b) $m = s = 2$; (c) $m = s = 3$; (d) $m = s = 4$; (e) $m = 1, s = 2$; (f) $m = 1, s = 3$; (g) $m = 2, s = 1$; (h) $m = 2, s = 3$.

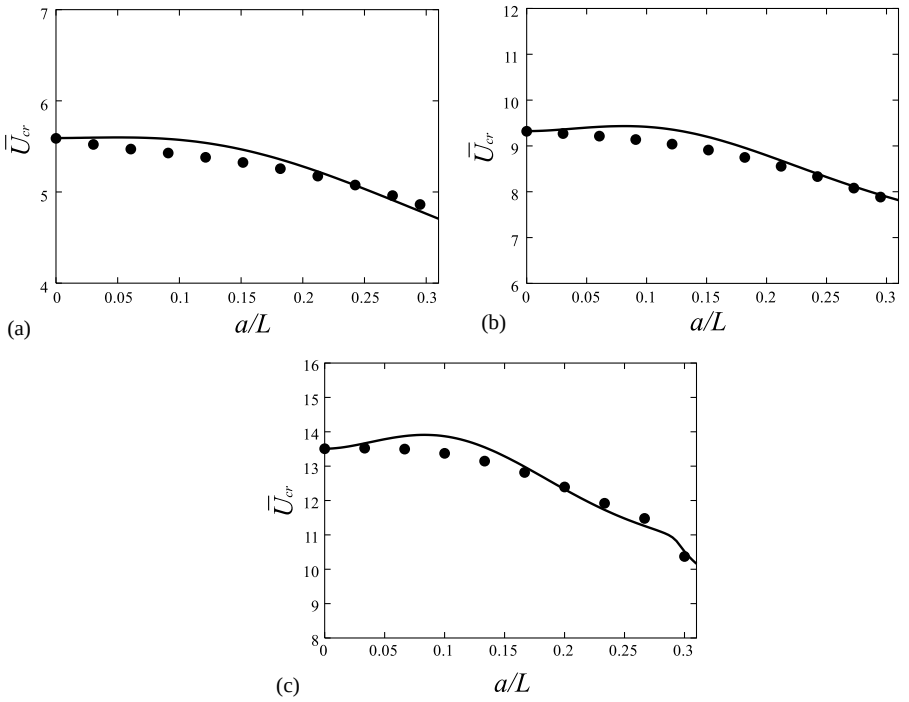

Fig. 4. Nondimensional critical flow speed $\bar{U}_{cr}$, at which dynamic instability is initiated, as function of the slenderness ratio a/L: —, the present method (49); ●, the Fourier transform method (52). (a) For the mass ratio $\beta = 0.2$; (b) for $\beta = 0.5$; (c) for $\beta = 0.8$.

Table 1
Critical flow speed $\bar{U}_{cr}$ as function of the number of terms S in the Galerkin expansion

	$(\beta = 0.2, \quad \bar{a} = 0.1)$		$(\beta = 0.2, \quad \bar{a} = 0.2)$		$(\beta = 0.8, \quad \bar{a} = 0.1)$		$(\beta = 0.8, \quad \bar{a} = 0.2)$	
S	Modal	Fourier	Modal	Fourier	Modal	Fourier	Modal	Fourier
2	5.3766	5.1572	5.0835	4.8348	—	—	—	—
4	5.5894	5.3796	5.2962	5.1534	14.8631	14.5922	12.7406	12.8166
6	5.5758	5.3885	5.2836	5.1718	14.2224	13.9291	12.4262	12.7835
8	5.5728	5.4013	5.2811	5.1908	13.9094	13.4831	12.3424	12.4829
10	5.5719	5.4140	5.2803	5.2088	13.8708	13.3736	12.3279	12.3947
12	5.5716	—	5.2801	—	13.8604	—	12.3238	—
14	5.5714	—	5.2800	—	13.8567	—	12.3222	—
16	5.5714	—	5.2799	—	13.8554	—	12.3216	—

some of the off-diagonal centrifugal force coefficients by moderate values of $\bar{a}$ (as seen in Fig. 3(f) and (g)) seems to be (moderately) transferred to the stability curves.

The reason why the poorly represented centrifugal force corresponding to the first modal coefficient, $Q^{(3)}_{111}$, does not seriously affect the critical flow speed predictions lies in the fact that the flutter mode is dominated by the higher modes (≥ 2) and only weakly associated with the lowest one. This is because a fluid–structure energy balance shows that the quantity $\overline{[\partial w/\partial x \cdot \partial w/\partial t]}_{x=L}$, where the overbar means the time average over one period of oscillation, must be equal to zero at the critical flow speed U_{cr}, and must be smaller than zero for $U > U_{cr}$ (Païdoussis, 1998, p. 64). Only the second and higher modes can ensure that $[\partial w/\partial x]_{x=L}$ has opposite sign of $[\partial w/\partial t]_{x=L}$ over most part of the vibration period. In fact, if the eigenvalue branches[2] $\lambda = \lambda(U)$ are numbered in ascending order according to the magnitude of their imaginary parts λ_I at $U = U_{cr}$, then, for moderate values of $\bar{a}$ at least, the onset of flutter occurs through the 'second branch' for $\beta = 0.2$, through the 'third branch' for $\beta = 0.5$, and through the 'fourth branch' for $\beta = 0.8$. By increasing β,

[2] See the discussion to Eq. (60).

more and more terms are needed in the Galerkin expansion in order to represent the critical branch properly (Païdoussis, 1998, p. 127).

7. Concluding remarks

This paper has proposed a modal expansion of the fluid velocity potential through application of the method of separation of variables and the Galerkin method. The validity of the approach has been checked by comparing the results with those obtained by the Fourier transform method. A major mathematical difficulty in the discretization of the equations of motion for a fluid-conveying shell is the coupling of fluid motion, described by a second-order differential equation, to structural motion which is described by a differential equation of fourth order. The Fourier transform method has clearly proved to be a powerful tool in connection with such problems. But very complex integrals which can only be evaluated numerically is a drawback. In contrast, any generalized fluid force term of the present method is very simple and explicit. The use of 'higher order' cantilever beam modal functions (which satisfy the natural boundary conditions involving second- and third-order derivatives) to expand the solution of a second-order differential equation is clearly a weak point. But although this affects the representation of the first mode in the centrifugal force matrix seriously, the unstable eigenvalue branches are not significantly affected, as the critical flow speeds predicted by the two methods agree well over a wide range of system parameters. In the light of this, it is concluded that the present modal expansion method is a useful simple alternative to the Fourier transform method in the analysis of dynamics and stability of cantilevered fluid-conveying shells and short beams.

It was decided from the outset to expand the potential in terms of the cantilever beam modal functions. This is a 'good' choice from a structural point of view. But the main results (39), (41), and (49) are applicable to any set of orthonormal functions, provided that the corresponding coefficients b_{mj}, c_{mj}, and d_{mj} (Eqs. (38) and (33), respectively) are evaluated and used. As a possible means of increasing the accuracy of the results, one could, instead of the beam modal functions, choose a set of functions with less 'structural priority' and higher 'fluid priority', such that the eigenfunctions (28) are better approximated. This can be achieved by constructing a set of orthogonal functions where the natural boundary conditions $f_m''(L) = f_m'''(L) = 0$ are relaxed (i.e., one or both are not satisfied).

Acknowledgements

Financial support from Aalborg University, Grundfos A/S, the Alexander von Humbolt Foundation, and the Danish Ministry of Information Technology and Research is gratefully acknowledged. We also wish to thank Mr. Max Hansen of Danfoss A/S for suggesting a technological problem which initiated the present work.

Appendix A. Expansion functions for the cantilevered tube

By using the nondimensional variable $\bar{x} = x/L$, and again drop the $^-$for convenience, the expansion functions (18) can be written as

$$\begin{aligned} f_m(x) &= \cosh(\kappa_m x) - \cos(\kappa_m x) - \sigma_m(\sinh(\kappa_m x) - \sin(\kappa_m x)) \\ &= \tfrac{1}{2}\{(1-\sigma_m)\mathrm{e}^{\kappa_m x} + (1+\sigma_m)\mathrm{e}^{-\kappa_m x} - (1+\mathrm{i}\sigma_m)\mathrm{e}^{\mathrm{i}\kappa_m x} - (1-\mathrm{i}\sigma_m)\mathrm{e}^{-\mathrm{i}\kappa_m x}\}, \end{aligned} \tag{A.1}$$

where the coefficients κ_m are the roots of

$$\cos\kappa\cosh\kappa + 1 = 0. \tag{A.2}$$

The first six roots are, approximately,

$$\kappa_1 = 1.87510407; \quad \kappa_2 = 4.69409113; \quad \kappa_3 = 7.85475744;$$

$$\kappa_4 = 10.99554073; \quad \kappa_5 = 14.13716839;$$

$$\kappa_6 = 17.27875953. \tag{A.3}$$

The coefficients σ_m are obtained from the expression

$$\sigma_m = \frac{\sinh \kappa_m - \sin \kappa_m}{\cosh \kappa_m + \cos \kappa_m} \tag{A.4}$$

which with $\kappa_1, \kappa_2, \ldots, \kappa_6$ inserted gives

$$\begin{aligned} &\sigma_1 = 0.734095514; \quad \sigma_2 = 1.018467319; \\ &\sigma_3 = 0.999224497; \quad \sigma_4 = 1.000033553; \\ &\sigma_5 = 0.999998550; \quad \sigma_6 = 1.000000063. \end{aligned} \tag{A.5}$$

The coefficients b_{mj} and c_{mj}, defined by Eqs. (38) and (33), respectively, are given by (Païdoussis and Issid, 1974; Païdoussis, 1998)

$$b_{mj} = \begin{cases} \dfrac{4}{(\kappa_j/\kappa_m)^2 + (-1)^{m+j}} & \text{for } m \neq j, \\ 2 & \text{for m = j,} \end{cases} \tag{A.6}$$

$$c_{mj} = \begin{cases} \dfrac{4(\kappa_m\sigma_m - \kappa_j\sigma_j)}{(-1)^{m+j} - (\kappa_j/\kappa_m)^2} & \text{for } m \neq j, \\ \kappa_m\sigma_m(2 - \kappa_m\sigma_m) & \text{for m = j.} \end{cases} \tag{A.7}$$

Appendix B. Proof of the identity $\sum_j b_{mj}\ b_{js} = c_{ms}$

From the definition of the coefficients b_{ms} and c_{ms} given in Eqs. (38) and (33), respectively, it follows that

$$\begin{aligned} c_{ms} &= \frac{1}{L}\int_0^L f_m'' f_s \,\mathrm{d}x = \frac{1}{L}\int_0^L \left(\frac{\mathrm{d}}{\mathrm{d}x} f_m'\right) f_s \,\mathrm{d}x \\ &= \frac{1}{L}\int_0^L \left(\frac{\mathrm{d}}{\mathrm{d}x}\sum_{j=1}^{\infty} b_{mj} f_j\right) f_s \,\mathrm{d}x = \frac{1}{L}\int_0^L \sum_{j=1}^{\infty} b_{mj} f_j' f_s \,\mathrm{d}x \\ &= \sum_{j=1}^{\infty} b_{mj} \frac{1}{L}\int_0^L f_j' f_s \,\mathrm{d}x = \sum_{j=1}^{\infty} b_{mj}\ b_{js}. \end{aligned} \tag{B.1}$$

References

Au-Yang, M.K., 1977. Generalized hydrodynamic mass for beam mode vibration of cylinders coupled by fluid gap. Journal of Applied Mechanics 44, 172–173.

Au-Yang, M.K., 1985. Flow-induced vibrations: Guidelines for design, diagnosis, and troubleshooting of common power plant components. *ASME* Journal of Pressure Vessel Technology 107, 326–334.

Au-Yang, M.K., 2001. Flow-Induced Vibration of Power and Process Plant Components: A Practical Workbook. ASME Press, New York.

Chen, S.-S., 1972. Free vibration of a coupled fluid/structural system. Journal of Sound and Vibration 21, 387–398.

Courant, R., Hilbert, D., 1953. Methods of Mathematical Physics, Vol. I. Interscience Publishers. New York.

Dowell, E.H., Widnall, S.E., 1966a. Generalized aerodynamic forces on an oscillating cylindrical shell: Subsonic and supersonic flow. AIAA Journal 4, 607–610.

Dowell, E.H., Widnall, S.E., 1966b. Generalized aerodynamic forces on an oscillating cylindrical shell. Quarterly of Applied Mathematics 24, 1–17.

Fujita, K., Ito, T., Kajii, S., 1991. Study on seismic response analysis, including fluid-structure interaction in a fast breeder reactor. In: *Proceedings of the 1st JSME/ASME Joint International Conference on Nuclear Engineering* (*ICONE-1*), *Tokyo, Japan*, JSME, Tokyo, pp. 197–202.

Kamke, E., 1967. Differentialgleichungen. Lösungsmethoden und Lösungen. Akademische Verlagsgesellschaft Geest & Portig K.-G, Leipzig.

Niordson, F.I.N., 1953. Vibrations of a cylindrical tube containing flowing fluid. Transactions of the Royal Institute of Technology, Stockholm, Sweden 73, 1–27.

Nguyen, V.B., Païdoussis, M.P., Misra, A.K., 1993. A new outflow model for cylindrical shells conveying fluid. Journal of Fluids and Structures 7, 417–419.

Païdoussis, M.P., Denise, J.-P., 1972. Flutter of thin cylindrical shells conveying fluid. Journal of Sound and Vibration 20, 9–26.

Païdoussis, M.P., Issid, N.T., 1974. Dynamic stability of pipes conveying fluid. Journal of Sound and Vibration 33, 267–294.

Païdoussis, M.P., Chan, S.P., Misra, A.K., 1984. Dynamics and stability of coaxial cylindrical shells containing flowing fluid. Journal of Sound and Vibration 97, 201–235.

Païdoussis, M.P., Luu, T.P., Laithier, B.E., 1986. Dynamics of finite-length tubular beams conveying fluid. Journal of Sound and Vibration 106, 311–331.

Païdoussis, M.P., 1987. Flow-induced instabilities of cylindrical structures. Applied Mechanics Reviews 40, 163–175.

Païdoussis, M.P., Li, G.X., 1993. Pipes conveying fluid: A model dynamical problem. Journal of Fluids and Structures 7, 137–204.

Païdoussis, M.P., 1998. Fluid-Structure Interactions. Slender structures and axial flow, Volume 1. Academic Press, London.

Pedley, T.J., Luo, X.Y., 1998. Modelling flow and oscillations in collapsible tubes. Theoretical and Computational Fluid Dynamics 10, 277–294.

Press, W.H., Teukolsky, S.A., Vetterling, W.T., Flannery, B.P., 1992. Numerical Recipes in Fortran. The Art of Scientific Programming, (2 Ed). Cambridge University Press, Cambridge.

Selmane, A., Lakis, A.A., 1997. Vibration analysis of anisotropic open cylindrical shells subjected to a flowing fluid. Journal of Fluids and Structures 11, 111–134.

Shayo, L.K., Ellen, C.H., 1974. The stability of finite length circular cross-section pipes conveying fluid. Journal of Sound and Vibration 37, 535–545.

Shayo, L.K., Ellen, C.H., 1978. Theoretical studies of internal flow-induced instabilities of cantilever pipes. Journal of Sound and Vibration 56, 463–474.

Widnall, S.E., Dowell, E.H., 1967. Aerodynamic forces on an oscillating cylindrical duct with an internal flow. Journal of Sound and Vibration 6, 71–85.

Zienkiewicz, O.C., Taylor, R.L., 1991. The Finite Element Method, Vol. 2. Solid and Fluid Mechanics and Non-linearity, 4th Edition, McGraw-Hill, London.